

Anisotropy in stability of electrodeposition at solid-solid interfaces and implications for metal anodes

Zeeshan Ahmad

Department of Mechanical Engineering, Carnegie Mellon University, Pittsburgh, Pennsylvania 15213, USA

Venkatasubramanian Viswanathan*

Department of Mechanical Engineering, Carnegie Mellon University, Pittsburgh, Pennsylvania 15213, USA and

Department of Physics, Carnegie Mellon University, Pittsburgh, Pennsylvania 15213, USA

(Dated: December 14, 2024)

We investigate the dynamics of electrodeposition at solid-solid interfaces with the materials exhibiting an anisotropic mechanical response. The stability of electrodeposition or resistance to formation of dendrites is studied within a linear stability analysis. The deformation and stress equations are solved using the Stroh formalism and faithfully recover the boundary conditions at the interface. The stability parameter is used to quantify the stability of different solid-solid interfaces incorporating the full anisotropy of the elastic tensor of the two materials. Results show a high degree of variability in the stability parameter depending on the crystallographic orientation of the solids in contact and points to opportunities for exploiting this effect in developing Li metal anodes.

I. INTRODUCTION

Solid-solid interfaces are ubiquitous in several important engineering applications like epitaxial thin films¹, solid-state batteries, solid oxide fuel cells, and is observed in nature in sedimentary rocks and porous materials with the formation of irregular interfaces called stylolites². In particular, electrodeposition at solid-solid interfaces is of great interest due to the possibility of obtaining safer and higher energy density batteries based on metal anodes. Controlling the growth of dendrites during electrodeposition at a solid electrolyte-metal interface could enable the use of metal anodes especially Li which rely on a plating rather than intercalation^{3,4}.

The key role of interfacial stresses in affecting the rates of electrodeposition was analyzed in a seminal work by Monroe and Newman⁵. They further analyzed the interfacial stability of Li/solid polymer electrolyte system within linear elasticity theory and showed using a kinetic model that solid polymer electrolytes with a sufficient modulus are capable of suppressing dendrite growth⁶. In a recent work, we extended the analysis to include the case of inorganic solid electrolytes.⁷ The key difference between a solid polymer electrolyte and a solid inorganic electrolyte is that they possess vastly different partial molar volume of lithium, which strongly affects the nature of hydrostatic stresses at the interface.⁷ We showed the existence of a new stable regime that is a density-driven stabilizing mechanism in addition to the pressure-driven stability mechanism identified earlier. However, both of these earlier analysis invoke the assumption of isotropic elastic response for the two solid materials. This assumption may generally not hold for the metal phase, Li since it has an anisotropy factor of 8.52,⁸ and the solid electrolyte phase⁹. Even for bulk isotropic materials, the local mechanical response may be anisotropic depending on the crystallographic orientation of the surfaces in contact¹. In this work, we relax this assumption

and analyze electrodeposition at solid-solid interfaces for anisotropic elastic materials.

In Ref. 7, we have shown a generalized stability diagram of electrodeposition for isotropic solid-solid interfaces. In this work, we develop a continuum mechanics-based theory for the analyzing stability of electrodeposition at interfaces with anisotropic mechanical response. The interface stability is studied using a linear stability analysis while incorporating the full anisotropy of the elastic tensor of the materials at the interface. The Stroh formalism used faithfully captures the boundary conditions of perturbation imposed in the linear stability analysis as well as vanishing of deformations and stresses far from the interface. The differences between the three cases of isotropic-isotropic, isotropic-anisotropic and fully anisotropic interface are highlighted through the deformation fields obtained and the stability diagrams. This paper is organized as follows. In Sec. II, we develop the treatment of anisotropy in the elastic tensor used throughout the paper. In Sec. III, we apply the Stroh formalism to solve deformation equations obtained on a linear perturbation. In Sec. IV, we generate stability diagrams and calculate the stability parameter which is a measure of stability. In Sec. V, we comment and discuss some general principles of stability diagrams obtained. We end with concluding remarks in Sec. VI.

II. THEORY

In this section, we develop the procedure used to compute the deformation and stress profiles for anisotropic materials including the crystallographic orientation dependent elastic matrix computations, and theory of electrodeposition at solid-solid interfaces.

A. Stroh Formalism

The Stroh formalism^{10,11}, based on the Eshelby-Read-Shockley formalism¹² is a mathematically powerful tool for solving two-dimensional problems in anisotropic linear elasticity. In what follows, we shall develop the Stroh formalism for a two-dimensional elasticity problem¹³ and explicitly write down the expressions for the deformation and stress fields in terms of the elastic tensor of the material.

We denote the deformation and stress fields by \mathbf{u} and $\boldsymbol{\sigma}$. For force balance, the necessary condition for the stress field is:

$$\text{div}(\boldsymbol{\sigma}) = \mathbf{0}. \quad (1)$$

The stress can be related to the deformation field using the linear elasticity relationship for anisotropic materials:

$$\sigma_{ij} = C_{ijkl}u_{k,l}. \quad (2)$$

Substituting the stress from Eq. (2) into the force balance and using the symmetries of $\boldsymbol{\sigma}$, we obtain:

$$C_{ijkl}u_{k,lj} = 0. \quad (3)$$

For the two-dimensional problem, Eq. (3) is a second order homogeneous differential equation in the independent variable x_1 and x_2 . The deformation \mathbf{u} will generically depend on a linear combination of x_1 and x_2 i.e. $\mathbf{u} = \mathbf{a}f(x_1 + px_2)$. Differentiating u_k with respect to x_l and x_j , and plugging in Eq. (3), we get

$$\begin{aligned} C_{ijkl}(\delta_{j1} + p\delta_{j2})(\delta_{l1} + p\delta_{l2})a_k &= 0 \quad (4) \\ \implies (C_{i1k1} + p(C_{i1k2} + C_{i2k1}) + p^2C_{i2k2}) a_k &= 0 \quad (5) \end{aligned}$$

In terms of the tensors $R_{ik} = C_{i1k1}$, $S_{ik} = C_{i1k2}$ and $T_{ik} = C_{i2k2}$, Eq. (5) becomes

$$\implies (\mathbf{R} + p(\mathbf{S} + \mathbf{S}^T) + p^2\mathbf{T}) \mathbf{a} = \mathbf{0}. \quad (6)$$

This is an eigen value equation with eigen value zero and eigen vector \mathbf{a} . For solutions to exist, we must have:

$$\det(\mathbf{R} + p(\mathbf{S} + \mathbf{S}^T) + p^2\mathbf{T}) = 0. \quad (7)$$

This gives a sixth degree equation which can be solved for p . The stress tensor associated with this deformation can be calculated using

$$\sigma_{i1} = (R_{ik} + pS_{ik})a_k f'(z) \quad (8a)$$

$$\sigma_{i2} = (S_{ki} + pT_{ik})a_k f'(z) \quad (8b)$$

The stress can be written in terms of the stress function φ :

$$\varphi_i = b_i f(x_1 + p_i x_2); \mathbf{b} = (\mathbf{S}^T + p\mathbf{T})\mathbf{a} = -\frac{1}{p}(\mathbf{R} + p\mathbf{S})\mathbf{a}$$

$$\sigma_{i1} = -\varphi_{i,2}, \sigma_{i2} = \varphi_{i,1} \quad (9)$$

The solutions to p will be complex with a non-zero imaginary part. Since the solutions will occur as complex conjugates, in the absence of degeneracies, we can write the deformation and stress as linear combinations of the individual solutions with $\text{Im}(p_\alpha) > 0$:

$$\mathbf{u} = 2\text{Re} \left\{ \sum_{\alpha=1}^3 q_\alpha \mathbf{a}_\alpha f_\alpha(x_1 + p_\alpha x_2) \right\} \quad (10a)$$

$$\varphi = 2\text{Re} \left\{ \sum_{\alpha=1}^3 q_\alpha \mathbf{b}_\alpha f_\alpha(x_1 + p_\alpha x_2) \right\} \quad (10b)$$

The above result may be written in compact form using the matrices $\mathbf{A} = [\mathbf{a}_1 \ \mathbf{a}_2 \ \mathbf{a}_3]$, $\mathbf{B} = [\mathbf{b}_1 \ \mathbf{b}_2 \ \mathbf{b}_3]$, $\mathbf{F} = \text{diag}[f(x_1 + p_1 x_2) \ f(x_1 + p_2 x_2) \ f(x_1 + p_3 x_2)]$ and constants $\mathbf{q} = [q_1 \ q_2 \ q_3]^T$:

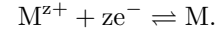
$$\mathbf{u} = 2\text{Re} \{ \mathbf{A}\mathbf{F}\mathbf{q} \} \quad (11a)$$

$$\varphi = 2\text{Re} \{ \mathbf{B}\mathbf{F}\mathbf{q} \} \quad (11b)$$

The procedure for degenerate case of isotropic material is mentioned in appendix A.

B. Electrodeposition at solid-solid interfaces

During electrodeposition, the metal ions present in the solid electrolyte are reduced at the metal anode according to the reaction:



The metal surface $x_2 = f(x_1, t)$ grows in response to current density i normal to the metal surface (Fig .1). The current density without any deformation can be related to the surface overpotential η_s through the Butler-Volmer equation:

$$\frac{i}{i_0} = \left[\exp\left(\frac{\alpha_a z F \eta_s}{RT}\right) - \exp\left(-\frac{\alpha_c z F \eta_s}{RT}\right) \right]. \quad (12)$$

Here α_a and α_c are the charge transfer coefficients associated with anodic and cathodic reactions, and i_0 is the exchange current density. The current density at a deformed interface can be written in terms of the undeformed current density as:

$$\frac{i_{\text{deformed}}}{i_{\text{undeformed}}} = \exp\left[\frac{(1 - \alpha_a)\Delta\mu_{e^-}}{RT}\right]. \quad (13)$$

where $\Delta\mu_{e^-}$ is the change in electrochemical potential of the electron due to deformation at the interface given by⁵:

$$\begin{aligned} \Delta\mu_{e^-} &= -\frac{V_M}{2z} (1 + v) (-\gamma\kappa \\ &\quad - \mathbf{e}_n \cdot [(\boldsymbol{\tau}_e - \boldsymbol{\tau}_s) \cdot \mathbf{e}_n]) \\ &\quad + \frac{V_M}{2z} (1 - v) (\Delta p_e + \Delta p_s). \end{aligned} \quad (14)$$

Here V_M is the molar volume of metal species in metallic form, $v = V_{M^{z+}}/V_M$ is ratio of molar volume of the metal

ion in the solid electrolyte to that in the metal, γ is the surface tension, κ is the mean curvature at the interface, $\boldsymbol{\tau}_e$ and $\boldsymbol{\tau}_s$ are the deviatoric stresses at the electrode and electrolyte sides of the interface, and Δp_e and Δp_s are the gage pressures at the electrode and electrolyte sides of the interface at $x_2 = 0$. Eq. (14) is obtained by calculating the electrochemical potential change $d\mu = (\partial\mu/\partial p)dp$ and using the equilibrium of Eq. (12)⁵. The negative sign in the deviatoric term is different from the positive sign obtained by Monroe and Newman⁵ since we use the convention of decomposition of stress as $-p\mathbf{I} + \boldsymbol{\tau}$, rather than $p\mathbf{I} + \boldsymbol{\tau}$ used by them.

The surface tension provides a stabilizing mechanism against roughening of the interface. It increases the electrochemical potential at peaks in the propagating interface and decreases it in the valleys. However, at length scales of roughening encountered in electrodeposition problems, the stabilization by surface tension is much smaller compared to that by interfacial stresses⁶. For this reason, we have ignored the contribution of surface tension term in the electrochemical potential throughout this paper.

Electrodeposition at solid-solid interfaces has several advantages compared to that at solid-liquid interfaces, especially for applications in batteries. Besides the stabilization of the propagating interface by interfacial stresses, solid electrolytes have a cation transference number close to 1. The mechanism of dendritic growth due to depletion of ions, common in liquid electrolytes, is thus not an issue when solid electrolytes are used.

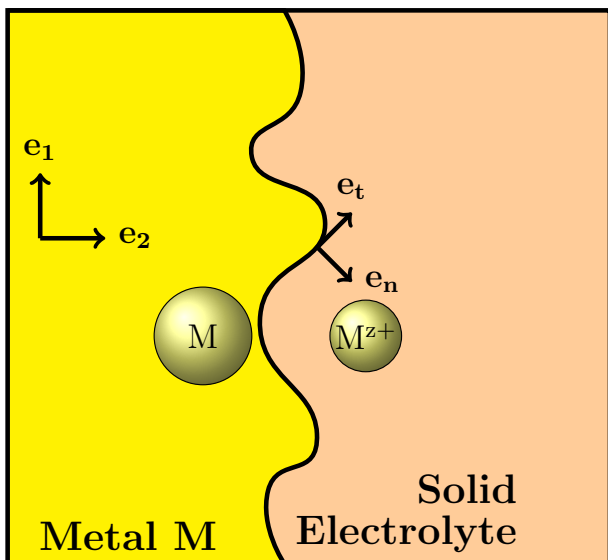


FIG. 1: (color online). Schematic of the electrodeposition problem with metal electrode-solid electrolyte interface. The metal surface $x_2 = f(x_1, t)$ grows on deposition of metal ions, the rate of which is proportional to the current. The local geometry alters the kinetics of deposition at the interface.

C. Transformation of the elastic tensor

For anisotropic analysis, the crystallographic directions of the electrode and electrolyte along \mathbf{e}_1 and \mathbf{e}_2 will determine the mechanical response through the elastic tensor. When the surfaces of the electrode and electrolyte in contact are such that the crystallographic axes of the material coincide with the actual axes (in Fig. 1), the elastic tensor can be plugged into the equations directly. This is the case when $[010]$ and $[100]$ crystallographic directions of the material are aligned along \mathbf{e}_2 and \mathbf{e}_1 respectively. If some other crystallographic directions are along \mathbf{e}_1 and \mathbf{e}_2 , the elastic tensor has to be transformed according to the rotation matrix \mathbf{Q} that aligns the required crystallographic directions along \mathbf{e}_1 and \mathbf{e}_2 as shown in Fig. 2. Once the rotation matrix \mathbf{Q} is obtained, the elastic tensor can be transformed according to:

$$\tilde{C}_{ijkl} = Q_{ip}Q_{jq}Q_{kr}Q_{ls}C_{pqrs} \quad (15)$$

An analogue of Eq. (15), given in appendix B, can be used to transform the elastic tensor in Voigt form as well.

Determination of \mathbf{Q} .—We have seen that the problem of determination of the elastic tensor reduces to determination of the rotation matrix \mathbf{Q} . Let $\mathcal{V}([hkl])$ denote the direction vector corresponding to crystallographic direction $[hkl]$. For example, $\mathcal{V}([100]) = (a, 0, 0)$ for a cubic crystal and $\mathcal{V}([111]) = (a, b, c)$ for an orthorhombic crystal where a , b and c are the respective lattice constants. For our calculations, we treated the crystallographic direction of the material along \mathbf{e}_2 , referred to as \mathbf{v}_2 , as the independent direction. Then, \mathbf{Q} is obtained as the rotation that aligns \mathbf{v}_2 along $\mathbf{v}_1 = \mathcal{V}([010])$ (Fig. 2). The transformation \mathbf{Q} is unique since it is a right-handed rotation about axis $\mathbf{v}_2 \times \mathbf{v}_1$ that transforms \mathbf{v}_2 to \mathbf{v}_1 . The new crystallographic direction along \mathbf{e}_1 , referred to as \mathbf{u}_2 is the dependent direction and can be obtained using: $\mathbf{u}_2 = \mathbf{Q}^{-1}\mathbf{u}_1$ where $\mathbf{u}_1 = \mathcal{V}([100])$. An example for a cubic crystal is shown in appendix B. Finally, we note that the elastic tensor depends not only on the crystallographic direction perpendicular to the interface (i.e. \mathbf{v}_2) but also on the crystallographic direction along \mathbf{e}_1 (i.e. \mathbf{u}_2).

III. LINEAR STABILITY ANALYSIS

A linear stability analysis can be used to determine the growth of various Fourier components of an arbitrary perturbation of the interface. It provides the boundary conditions to the deformation problem. Initially, the electrode is located at $x_2 < 0$ and the electrolyte at $x_2 > 0$. The solids are assumed to be in contact at all times i.e. $\mathbf{u}_e(x_1, 0) = \mathbf{u}_s(x_1, 0)$. Additionally, all deformations are assumed to vanish far from the interface i.e. $\lim_{x_2 \rightarrow \pm\infty} \mathbf{u}(x_1, x_2) = \mathbf{0}$. The interface $x_2 = 0$ between the solids is perturbed in a sinusoidal fashion:

$$(x_1, 0) \mapsto (x_1, A \cos(kx_1)) \quad (16)$$

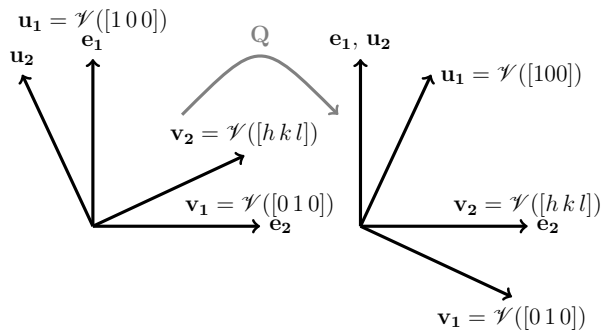


FIG. 2: Transformation of the elastic tensor for anisotropic analysis. The rotation bring the required crystallographic directions \mathbf{v}_2 and \mathbf{u}_2 along \mathbf{e}_2 and \mathbf{e}_1 . Note that the rotation operation is performed on the crystallographic axes of the material and not on the actual axes considered in the problem \mathbf{e}_1 and \mathbf{e}_2 .

To obtain a sinusoidal perturbation of the interface, we try the following ansatz for the functions f_α in Eq. (10):

$$f_\alpha(x_1 + p_\alpha x_2) = \begin{cases} e^{ik(x_1 + p_\alpha x_2)} & x_2 > 0 \\ e^{-ik(x_1 + p_\alpha x_2)} & x_2 < 0 \end{cases} \quad (17)$$

Here p_α are solutions of the sixth degree equation obtained from Eq. (7). Since p_α are imaginary, the term $e^{\pm ip_\alpha x_2}$ represents the decay of the perturbation as we move away from the interface. A straightforward calculation of \mathbf{u} shows that the deformation obtained using this ansatz gives the required perturbation, while also vanishing far from the interface. A tangential force balance at the interface is also imposed:

$$\mathbf{e}_t \cdot \boldsymbol{\tau}_e \mathbf{e}_n = \mathbf{e}_t \cdot \boldsymbol{\tau}_s \mathbf{e}_n. \quad (18)$$

To assess the stability of electrodeposition, we solved for the deformations and stresses and computed $\Delta\mu_e$ using Eq. (14). From linear stability analysis, $\Delta\mu_e(x_1)$ has a form similar to the perturbation i.e. $\Delta\mu_e(x_1) = \chi \cos(kx_1)$. From Eq. (13), we see that the current will promote roughening when $\chi > 0$ and reduce roughening when $\chi < 0$. This analysis is quite similar to that of Asaro and Tiller for instability during stress corrosion cracking with different kinetics of growth¹⁴. A similar result exists for the stability of stressed interface¹. The interface is stable if the chemical potential of the material increases in the direction of growth. The condition $\chi < 0$ ensures that the chemical potential of the electron at peaks is lower so that the mass transfer of Li is lower at the peaks.

Fig. 3 shows the deformation profiles obtained for three different classes of electrode-electrolyte interfaces: both isotropic, electrolyte isotropic and electrode anisotropic, and both anisotropic on the application of a sinusoidal perturbation at the interface. We observe qualitative differences in the deformation profiles for the three cases. The rate of decay of deformation, which depends on the solutions p_α through Eq. (17), are different

due to the different mechanical responses. This can be seen from the variation in deformations at the boundaries (i.e. as we move away from interface $x_2 = 0$) of the three cases in Fig. 3.

IV. RESULTS

A. Isotropic-isotropic interface

In this case, the stability parameter can be expressed analytically in terms of the mechanical properties (G, ν) of the electrode and electrolyte and parameters (V_M, v, z). The stability diagram has four regions out of which two are stable⁷. These are high density low shear modulus region, whose stability is density-driven and low density high shear modulus region, whose stability is pressure driven. The details can be found in Ref. 7. The stability of low density high shear modulus region was first predicted by Monroe and Newman⁶ and later verified experimentally by Balsara and co-workers^{15,16}. In our study, we solved the deformation equations using the Stroh formalism for the degenerate case of isotropic material as shown in Appendix A. The results obtained for the stability parameter were the same as Ref. 6 and 7, thus validating our use of the machinery of Stroh formalism.

B. Isotropic-Anisotropic interface

This interface has an anisotropic electrode on one side and isotropic solid electrolyte on the other. This is worth studying since the candidate material for anode, namely Li metal is highly anisotropic compared to other materials⁸. Fig. 4 shows the value of the stability parameter χ for the three cases of [100], [110] and [111] crystallographic direction of Li perpendicular to the surface of solid electrolyte as a function of its shear modulus. As observed in the isotropic-isotropic case, for $v < 1$, χ increases with G_s resulting in stability below the critical shear modulus value. For $v > 1$, χ decreases with G_s , resulting in stability beyond a critical shear modulus. Each surface of Li has a different elastic response which results in different stresses at the interface. The stress results in different values of the stability parameter χ for the different surfaces. The stability diagram is then dependent on surface orientation of Li in contact with the solid electrolyte. Fig. 5 shows the stability diagram for different surfaces of Li metal anode in contact with a solid electrolyte. The nature of the stability diagram remains the same with two stable and two unstable regions. However, the critical shear modulus curves shift depending on the specific surface of Li in contact with the solid electrolyte. In the $v > 1$ region, for example, the surface (111) imposes stronger requirements on the shear modulus for stability than the (100) surface. This presents opportunities for dendrite suppression if solid

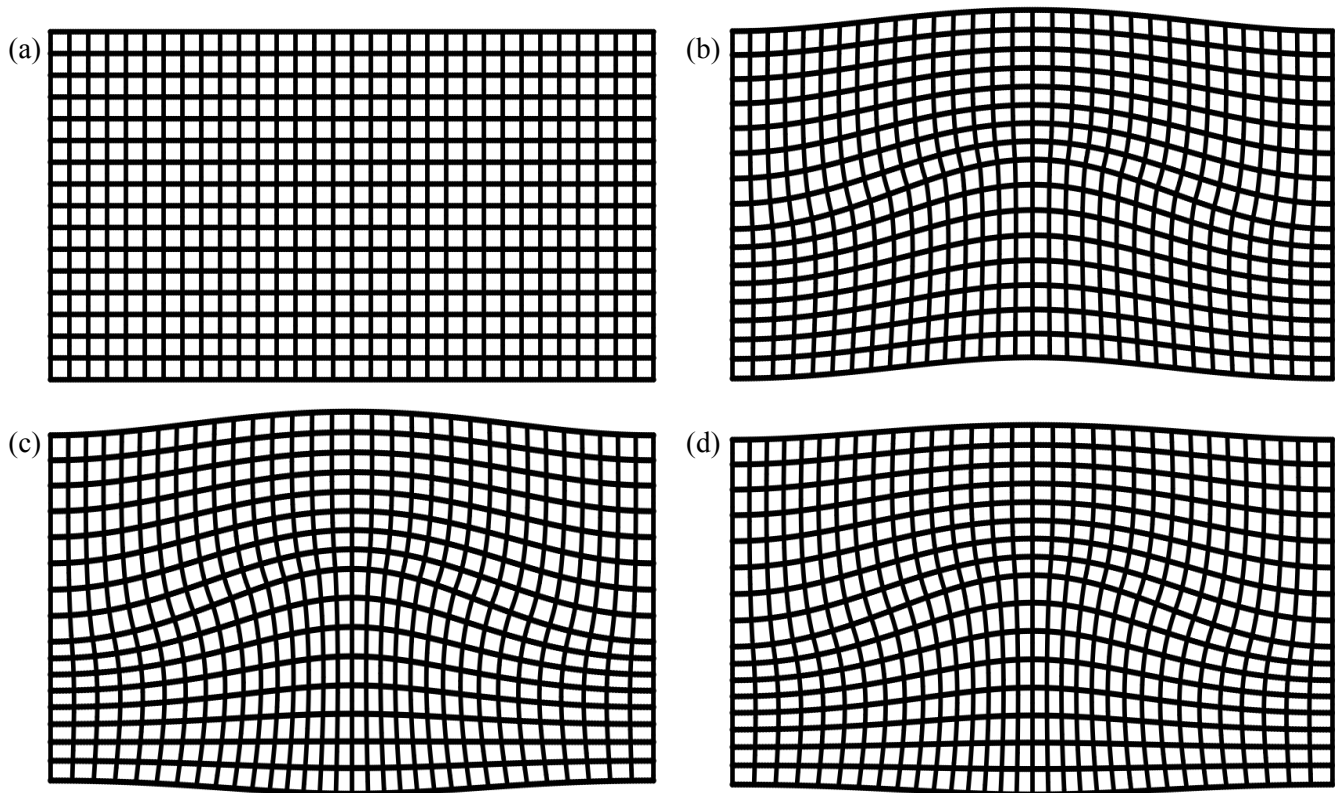


FIG. 3: (a) Initial position and deformed positions for different interfaces on application of a sinusoidal perturbation: (b) isotropic-isotropic, (c) isotropic-anisotropic and (d) anisotropic-anisotropic interface. The interface $x_2 = 0$ is located in the middle with electrolyte above ($x_2 > 0$) and electrode below ($x_2 < 0$). The interface materials are: Li-LiI with (c) (010) Li surface in contact with isotropic LiI, (d) (010) Li surface with (010) LiI surface with $\mathbf{v}_2 = \mathcal{V}([010])$, $\mathbf{u}_2 = \mathcal{V}([100])$ as in Fig. 2.

electrolytes could be made to preferentially comply along certain directions, for example, $[111]$.

C. Anisotropic-anisotropic interface

The fully anisotropic interface equations were solved using the Stroh formalism with the stresses and deformations obtained using Eq. (11). The orientation dependent elastic tensor of the two materials enters the problem through eigen vectors \mathbf{a} , \mathbf{b} and solutions p of the sextet Eq. (7). Due to the high dimensionality of the anisotropic problem (21 components of the elastic tensor, different surfaces in contact) and the absence of an analytical solution for the stability parameter, we assessed the stability of electrodeposition at anisotropic-anisotropic interfaces on a case by case basis instead of a high dimensional stability diagram. We considered several high Li-ion conducting solids including several obtained by Sendek et al. through large-scale screening of Li-containing compounds¹⁷ which have experimental¹⁸ or first-principles computed elastic tensor available^{9,19,20}. Overall, the solid electrolytes considered here include the

major classes of thiophosphates ($\text{Li}_{10}\text{GeP}_2\text{S}_{12}$), halides (LiI), garnets ($\text{Li}_5\text{La}_3\text{Ta}_2\text{O}_{12}$), phosphates (Li_3PO_4), sulfides (Li_2S) and alloys (LiCu_3). Low index surfaces of Li and solid electrolyte were considered at the interface.

Table I lists the values of the stability parameter χ for different interfaces between Li metal anode and a solid electrolyte. The crystallographic directions along \mathbf{e}_1 and \mathbf{e}_2 are \mathbf{u}_2 and \mathbf{v}_2 for the two materials in contact. The molar volume ratio v was calculated using the procedure mentioned in Ref. 7. The role of anisotropy is evident through the drastic changes in the stability parameter upon changing the interface crystallographic directions. Inorganic solid electrolytes with a lower shear modulus generally have lower stability parameters as should be expected from the isotropic case for $v < 1$. Unfortunately, none of the solid electrolytes we investigated have a negative stability parameter i.e. an interface stable against growth of dendrites.

The volume ratio v here deserves some discussion. Inorganic solid electrolytes generally have $0 < v < 1$. Li alloys have v close to 1 while compounds with low Li coordination number have lower v . If we observe the overall range of χ for different materials while varying surface

TABLE I: Stability parameter of fully anisotropic Li-solid electrolyte interfaces. The crystallographic orientation of the solids can be identified from crystallographic directions \mathbf{u}_2 and \mathbf{v}_2 which are lie along \mathbf{e}_1 and \mathbf{e}_2 respectively.

Electrolyte material	Electrode \mathbf{v}_2	Electrode \mathbf{u}_2	Electrolyte \mathbf{v}_2	Electrolyte \mathbf{u}_2	χ (kJ/mol-nm)
Li ₁₀ GeP ₂ S ₁₂ $v = 0.151$	[0 1 0]	[1 0 0]	[0 1 0]	[1 0 0]	7524.5
	[1 1 0]	[1 $\bar{1}$ 0]	[0 1 0]	[1 0 0]	10990.3
	[0 1 1]	[1 0 0]	[0 1 0]	[1 0 0]	7781.1
	[1 1 1]	[79 58 21]	[0 1 0]	[1 0 0]	9161.7
	[0 1 0]	[1 0 0]	[1 1 0]	[1 $\bar{1}$ 0]	7609.6
	[0 1 0]	[1 0 0]	[1 1 1]	[95 56 19]	8348.0
	[1 1 0]	[1 $\bar{1}$ 0]	[1 1 0]	[1 $\bar{1}$ 0]	11075.4
	[0 1 0]	[1 0 0]	[0 0 1]	[1 0 0]	10234.9
	[1 1 0]	[1 $\bar{1}$ 0]	[0 0 1]	[1 0 0]	14898.8
LiI $v = 0.099$	[0 1 0]	[1 0 0]	[0 1 0]	[1 0 0]	6525.4
	[1 1 0]	[1 $\bar{1}$ 0]	[0 1 0]	[1 0 0]	10776.0
	[1 1 1]	[79 58 21]	[0 1 0]	[1 0 0]	8526.9
	[0 1 0]	[1 0 0]	[1 1 0]	[1 $\bar{1}$ 0]	6619.8
	[0 1 0]	[1 0 0]	[1 1 1]	[79 58 21]	7530.8
	[0 1 0]	[1 0 0]	[0 1 1]	[1 0 0]	7903.4
	[1 1 0]	[1 $\bar{1}$ 0]	[1 1 0]	[1 $\bar{1}$ 0]	10870.5
	[1 1 0]	[1 $\bar{1}$ 0]	[1 1 1]	[79 58 21]	11950.4
Li ₅ La ₃ Ta ₂ O ₁₂ $v = 0.085$	[0 1 0]	[1 0 0]	[0 1 0]	[1 0 0]	44897.9
	[1 1 0]	[1 $\bar{1}$ 0]	[0 1 0]	[1 0 0]	50014.9
	[1 1 1]	[79 58 21]	[0 1 0]	[1 0 0]	47980.7
	[0 1 0]	[1 0 0]	[1 1 0]	[1 $\bar{1}$ 0]	44924.5
	[0 1 0]	[1 0 0]	[1 1 1]	[79 58 21]	46113.1
	[0 1 0]	[1 0 0]	[0 1 1]	[1 0 0]	46583.4
	[1 1 0]	[1 $\bar{1}$ 0]	[1 1 0]	[1 $\bar{1}$ 0]	50041.5
	[1 1 0]	[1 $\bar{1}$ 0]	[1 1 1]	[79 58 21]	51257.6
Li ₃ PO ₄ $v = 0.098$	[0 1 0]	[1 0 0]	[0 1 0]	[1 0 0]	35942.7
	[1 1 0]	[1 $\bar{1}$ 0]	[0 1 0]	[1 0 0]	41575.6
	[0 1 1]	[1 0 0]	[0 1 0]	[1 0 0]	36586.7
	[1 1 1]	[79 58 21]	[0 1 0]	[1 0 0]	39221
	[0 1 0]	[1 0 0]	[1 1 0]	[78 51 0]	35466.1
	[0 1 0]	[1 0 0]	[1 1 1]	[90 31 10]	35136.1
	[0 1 0]	[1 0 0]	[0 1 1]	[1 0 0]	35671.5
	[0 1 0]	[1 0 0]	[1 0 0]	[0 1 0]	34696.9
Li ₂ S $v = 0.066$	[0 1 0]	[1 0 0]	[0 1 0]	[0 1 0]	26619.8
	[1 1 0]	[1 $\bar{1}$ 0]	[1 1 0]	[1 1 0]	32705.2
	[0 1 1]	[1 0 0]	[0 1 1]	[0 1 1]	27536.2
	[1 0 1]	[50 71 50]	[1 0 1]	[1 0 1]	31769.4
	[1 1 1]	[79 58 21]	[1 1 1]	[1 1 1]	30338.8
	[0 1 0]	[1 0 0]	[0 1 0]	[0 1 0]	26637.4
	[0 1 0]	[1 0 0]	[0 1 0]	[0 1 0]	27666.1
	[0 1 0]	[1 0 0]	[0 1 0]	[0 1 0]	27216.4
LiCu ₃ $v = 0.738$	[0 1 0]	[1 0 0]	[0 1 0]	[1 0 0]	8005.3
	[1 1 0]	[1 $\bar{1}$ 0]	[0 1 0]	[1 0 0]	11995.8
	[0 1 1]	[1 0 0]	[0 1 0]	[1 0 0]	10457.7
	[1 1 1]	[79 58 21]	[0 1 0]	[1 0 0]	11628.6
	[0 1 0]	[1 0 0]	[1 1 0]	[1 $\bar{1}$ 0]	9910.0
	[0 1 0]	[1 0 0]	[1 1 1]	[95 56 19]	14296.6
	[1 1 0]	[1 $\bar{1}$ 0]	[1 1 0]	[1 $\bar{1}$ 0]	13900.5
	[0 1 0]	[1 0 0]	[0 0 1]	[1 0 0]	11148.1
[1 1 0]	[1 $\bar{1}$ 0]	[0 0 1]	[1 0 0]	15682.2	

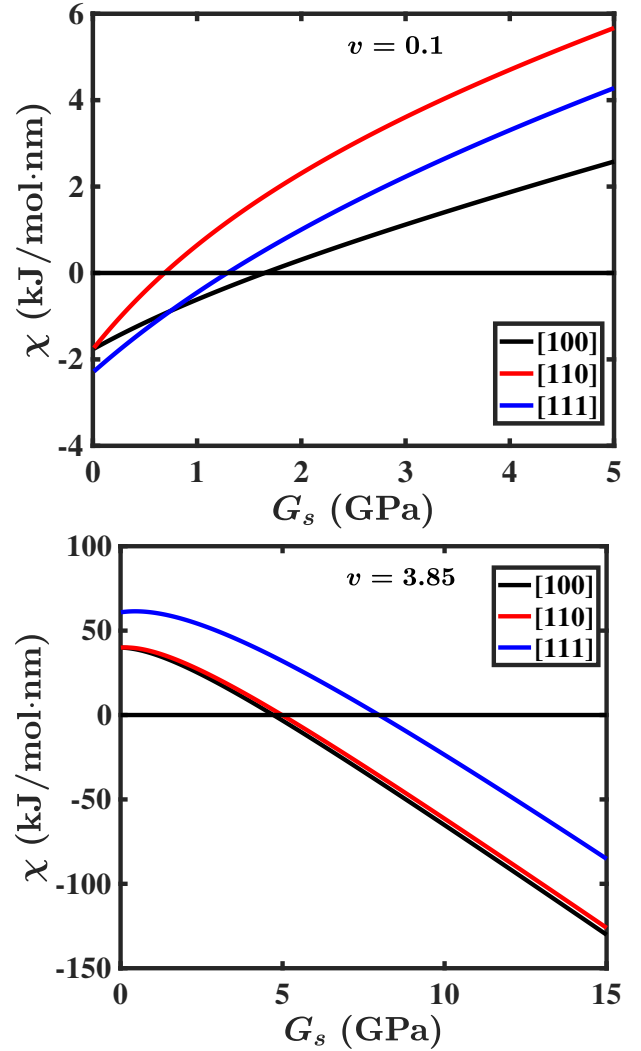


FIG. 4: (color online). Stability parameter as a function of shear modulus of solid electrolyte for $\mathbf{v}_2 = \mathcal{V}([0 1 0])$, $\mathcal{V}([1 1 0])$ and $\mathcal{V}([1 1 1])$ and $v = 0.1$, 3.85 respectively..

orientations, Li₁₀GeP₂S₁₂ and LiI with low shear modulus have stability parameter closer to zero than the other high shear modulus compounds, while alloy LiCu₃ with high volume ratio v has χ closer to zero despite a high shear modulus (36 GPa). On comparing χ for different surface orientations for a given material, we observe that the orientation with $\mathbf{v}_2 = \mathcal{V}([0 1 0])$ and $\mathbf{u}_2 = \mathcal{V}([1 0 0])$ for both the electrode and electrolyte (first entry in the table for each material) has the lowest stability parameter. This is, thus, the most compliant arrangement.

V. DISCUSSION

We discuss some general principles which can be used to make sense of the stability diagrams. For the isotropic case, the deviatoric term in the electrochemical potential

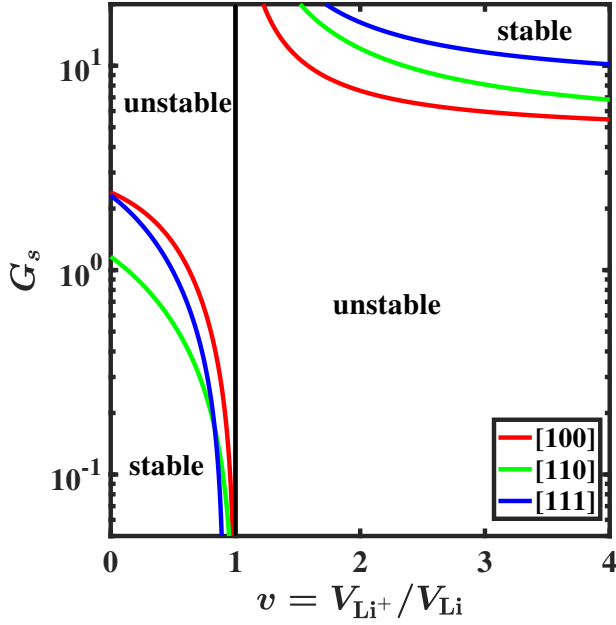


FIG. 5: (color online). Stability diagram for $\mathbf{v}_2 = \mathcal{V}([100])$, $\mathcal{V}([110])$ and $\mathcal{V}([111])$ showing the range of shear moduli over which electrodeposition is stable and its dependence on the volume ratio v of the cation and metal atom.

is always destabilizing. The existence of stability regions for isotropic solid electrolyte case follows from the dependence of stability parameter χ on the hydrostatic term alone. χ represents the electrochemical potential change of the electron at a peak in the interface ($\Delta\mu_{e^-} = \chi$ when $\cos(kx_1) = 1$). For $v < 1$, the hydrostatic term in Eq. (14) is stabilizing when $\Delta p_e + \Delta p_s$ is negative. At the peak (e.g. $x = 0$), tensile stress is generated at the electrode side of the interface and compressive at the electrolyte side, resulting in $\Delta p_e < 0$ and $\Delta p_s > 0$. When G_s is low, $|\Delta p_s| \ll |\Delta p_e|$ which will make this term stabilizing. For $v > 1$, we require $\Delta p_e + \Delta p_s > 0$ for stability and this will occur at high G_s with $|\Delta p_s| \gg |\Delta p_e|$. This argument explains the stable regimes at the bottom left and top right in Fig. 5. The two unstable regions in the isotropic-isotropic and isotropic-anisotropic cases are separated by the black line and are different phases since one cannot go from one phase to another without passing through $\chi = 0$.

VI. CONCLUSIONS

We used the Stroh formalism to analyze the stability of electrodeposition at different kinds of solid-solid interfaces. The results obtained for the isotropic case using this formalism match the results of previous studies. For completely anisotropic interfaces, we find that the stability parameter is highly dependent on the crystallographic orientation of the solids in contact. In the context of Li

metal anodes in contact with electrolyte having $\nu > 1$, compliance along $[100]$ direction for a solid electrolyte leads to less stringent requirements on the modulus of the solid electrolyte while $[111]$ leads to more stringent requirements. A similar analysis might be useful in problems on stability of solid-solid interfaces encountered in other areas, for example, epitaxial thin films when the materials have a high degree of anisotropy.

ACKNOWLEDGMENTS

We thank Srivatsan Hulikal for helpful discussions. Z. A. acknowledges support from the ARPA-E Integration and Optimization of Novel Ion Conducting Solids (IONICS) program under award number DE-AR0000774. Z. A. and V. V. gratefully acknowledge support from the U.S. Department of Energy, Energy Efficiency and Renewable Energy Vehicle Technologies Office under award number DE-EE0007810.

Appendix A: Stroh Formalism for degenerate case of isotropic material

For isotropic materials with shear modulus G Poisson's ratio ν , all three solutions p_α of Eq. (7) are equal to i . The matrices \mathbf{F} , \mathbf{A} and \mathbf{B} used to determine to the solution are:

$$\mathbf{F} = \begin{bmatrix} f(x_1 + p_1 x_2) & x_2 f'(x_1 + p_1 x_2) & 0 \\ 0 & f(x_1 + p_2 x_2) & 0 \\ 0 & 0 & f(x_1 + p_3 x_2) \end{bmatrix}$$

$$\mathbf{A} = \psi \begin{bmatrix} 1 & -i\gamma & 0 \\ i & -\gamma & 0 \\ 0 & 0 & \varepsilon \end{bmatrix}; \mathbf{B} = \begin{bmatrix} 2i & 1 & 0 \\ -2 & -i & 0 \\ 0 & 0 & i\varepsilon \end{bmatrix}$$

$$\psi = \frac{1}{\sqrt{8G(1-\nu)}}, \gamma = \frac{1}{2}(3-4\nu), \varepsilon = (1-i)\sqrt{2(1-\nu)}$$

Eq. (10) can then be used to obtain deformation and stress fields for isotropic materials.

Appendix B: Transformation of elastic tensor in Voigt form

Let \mathbf{C} be the 6×6 elastic tensor in Voigt form associated with a particular coordinate system and $\tilde{\mathbf{C}}$ be the transformed elastic tensor under rotation \mathbf{Q} . Then $\tilde{\mathbf{C}}$ can be calculated as^{13,21}:

$$\tilde{\mathbf{C}} = \mathbf{KCK}^T \quad (\text{B1})$$

where \mathbf{K} is 6×6 tensor given by:

$$\begin{aligned} \mathbf{K} &= \begin{bmatrix} \mathbf{K}_1 & 2\mathbf{K}_2 \\ \mathbf{K}_3 & \mathbf{K}_4 \end{bmatrix} \\ [\mathbf{K}_1]_{ij} &= [\mathbf{Q}]_{ij}^2 \\ [\mathbf{K}_2]_{ij} &= [\mathbf{Q}]_{i \bmod(j+1,3)} [\mathbf{Q}]_{i \bmod(j+2,3)} \\ [\mathbf{K}_3]_{ij} &= [\mathbf{Q}]_{\bmod(i+1,3)j} [\mathbf{Q}]_{\bmod(i+2,3)j} \\ [\mathbf{K}_4]_{ij} &= [\mathbf{Q}]_{\bmod(i+1,3)\bmod(j+1,3)} [\mathbf{Q}]_{\bmod(i+2,3)\bmod(j+2,3)} \\ &\quad + [\mathbf{Q}]_{\bmod(i+1,3)\bmod(j+2,3)} [\mathbf{Q}]_{\bmod(i+2,3)\bmod(j+1,3)} \end{aligned}$$

where

$$\text{mod}(i, j) = \begin{cases} i & i \leq 3 \\ i - 3 & i > 3 \end{cases}$$

Next, we show how to determine the rotation matrix \mathbf{Q} and \mathbf{u}_2 given \mathbf{v}_2 .

Example for a cubic crystal.- Let \mathbf{v}_2 coincide with $[110]$ direction of the crystal or $\mathbf{v}_2 = \mathcal{V}([110])$. Then the rota-

tion matrix \mathbf{Q} obtained by following the procedure mentioned in Sec. II C is given by:

$$\mathbf{Q} = \begin{bmatrix} \frac{1}{\sqrt{2}} & -\frac{1}{\sqrt{2}} & 0 \\ \frac{1}{\sqrt{2}} & \frac{1}{\sqrt{2}} & 0 \\ 0 & 0 & 1 \end{bmatrix}$$

The crystallographic direction which aligns along \mathbf{e}_1 due to this rotation is given by:

$$\mathbf{u}_2 = \mathbf{Q}^{-1} \mathcal{V} \left(\begin{bmatrix} 1 \\ 0 \\ 0 \end{bmatrix} \right) = a \begin{bmatrix} \frac{1}{\sqrt{2}} \\ -\frac{1}{\sqrt{2}} \\ 0 \end{bmatrix} = \mathcal{V}([1\bar{1}0])$$

Hence, \mathbf{u}_2 corresponds to the $[1\bar{1}0]$ direction of the crystal. Similarly, the other combinations $(\mathbf{v}_2, \mathbf{u}_2)$ along $(\mathbf{e}_2, \mathbf{e}_1)$ are $([011], [100])$, $([221], [11\bar{1}0\bar{2}])$. Note that \mathbf{u}_2 is always perpendicular to \mathbf{v}_2 . For non-cubic crystals, care must be taken to differentiate the crystallographic axes (in miller index notation) from the actual direction vectors for calculating \mathbf{Q} and \mathbf{u}_2 .

* venkvis@cmu.edu

¹ L. B. Freund and S. Suresh, *Thin Film Materials: Stress, Defect Formation and Surface Evolution* (Cambridge University Press, Cambridge, 2004).

² L. Angheluta, E. Jettestuen, J. Mathiesen, F. Renard, and B. Jamtveit, *Phys. Rev. Lett.* **100**, 096105 (2008).

³ W. Xu, J. Wang, F. Ding, X. Chen, E. Nasybulin, Y. Zhang, and J.-G. Zhang, *Energy Environ. Sci.* **7**, 513 (2014).

⁴ O. Sapunkov, V. Pande, A. Khetan, C. Choomwattana, and V. Viswanathan, *Transl. Mater. Res.* **2**, 045002 (2015).

⁵ C. Monroe and J. Newman, *J. Electrochem. Soc.* **151**, A880 (2004).

⁶ C. Monroe and J. Newman, *J. Electrochem. Soc.* **152**, A396 (2005).

⁷ Z. Ahmad and V. Viswanathan, arXiv:1702.08406 *Phys. Rev. Lett.* (to be published).

⁸ C. Xu, Z. Ahmad, A. Aryanfar, V. Viswanathan, and J. R. Greer, *Proc. Natl. Acad. Sci. USA* **114**, 57 (2017).

⁹ Z. Ahmad and V. Viswanathan, *Phys. Rev. B* **94**, 064105 (2016).

¹⁰ A. N. Stroh, *Philos. Mag.* **3**, 625 (1958).

¹¹ A. N. Stroh, *J. Math. Phys.* **41**, 77 (1962).

¹² J. Eshelby, W. Read, and W. Shockley, *Acta Metall.* **1**, 251 (1953).

¹³ T. C. T. Ting, *Anisotropic elasticity* (Oxford University Press, New York, 1996).

¹⁴ R. J. Asaro and W. A. Tiller, *Metall. Trans.* **3**, 1789 (1972).

¹⁵ G. M. Stone, S. A. Mullin, A. A. Teran, D. T. Hallinan, A. M. Minor, A. Hexemer, and N. P. Balsara, *J. Electrochem. Soc.* **159**, A222 (2012).

¹⁶ K. J. Harry, K. Higa, V. Srinivasan, and N. P. Balsara, *J. Electrochem. Soc.* **163**, A2216 (2016).

¹⁷ A. D. Sendek, Q. Yang, E. D. Cubuk, K.-A. N. Duerloo, Y. Cui, and E. J. Reed, *Energy Environ. Sci.* (2017).

¹⁸ H. P. R. Frederikse, in *Handbook of Chemistry and Physics*, edited by D. Lide (CRC Press Taylor and Francis, Boca Raton, 2008) 88th ed.

¹⁹ A. Jain, S. P. Ong, G. Hautier, W. Chen, W. D. Richards, S. Dacek, S. Cholia, D. Gunter, D. Skinner, G. Ceder, and K. A. Persson, *APL Mater.* **1**, 011002 (2013).

²⁰ M. De Jong, W. Chen, T. Angsten, A. Jain, R. Notestine, A. Gamst, M. Sluiter, C. K. Ande, S. Van Der Zwaag, J. J. Plata, *et al.*, *Sci. Data* **2**, 150009 (2015).

²¹ A. F. Bower, *Applied mechanics of solids* (CRC press, Boca Raton, FL, 2009).